Bulletin of Earthquake Engineering
https://doi.org/10.1007/s10518-026-02529-2

ORIGINAL ARTICLE

Behavior of reinforced concrete columns under axial load, bending, and torsional combined loading

Salih Cengiz[1] · Mehmet Kamanli[1] · Alptug Unal[1] · Abdulkadir Solak[1] · Baris Binici[2]

Received: 4 February 2026 / Accepted: 23 May 2026
© The Author(s) 2026

Abstract
In this study, the lateral cyclic response of ten reinforced concrete columns subjected to constant axial load and torsion was experimentally investigated. The parameters of the study were the axial load ratio, torsional rotation/lateral drift ratio, and stirrup spacing. It was observed that torsional moments can significantly reduce the energy dissipation capacity, displacement ductility and plastic rotation capacity while increasing the plastic hinge length. The axial load, torsion and bending interactions computed with models available in the literature were compared with the test results. Using the experimental data, a modification to the existing interaction model was proposed. The plastic rotation capacities of the tested columns were compared with the limits in the Turkish Earthquake Code-2018 and ASCE SEI-2017 neglecting the influence of torsion. Based on the observations, it is found that neglecting torsion induced rotations can be unsafe in performance assessment of reinforced concrete columns.

Keywords Interaction model · Plastic hinge · Plastic rotation · Reinforced concrete column · Torsion

Notation List

b	Column section width
d’	Concrete cover

✉ Salih Cengiz
scengiz@ktun.edu.tr

Mehmet Kamanli
mkamanli@ktun.edu.tr

Alptug Unal
aunal@ktun.edu.tr

Abdulkadir Solak
abdulkadirsolak@ktun.edu.tr

Baris Binici
binici@metu.edu.tr

[1] Konya Technical University, Konya, Türkiye

[2] Middle East Technical University, Ankara, Türkiye

Published online: 03 June 2026

d_b	Rebar diameter
EI_{eff}	Effective stiffness
EI_g	Gross stiffness
F	Force applied to the beam ends on the column
f'_c	Concrete compressive strength
H	Column height
h	Column section depth
k_e	confinement effectiveness coefficient
LC	Load-cell
LVDT	Linear variable differential transformer
L	Shear span
L_p	Plastic hinge length
L_s	Shear span length
M	Bending moment
M_0	Ultimate bending moment in pure bending
$M_{0.004}$	Moment at which concrete compressive strain reached 0.004
M_w	Moment magnitude
N	Axial load
N_0	Axial load in pure compression
n	Axial load ratio
P	Lateral force
r	Rotation/drift ratio
s	Stirrup spacing
T	Torsion
T_0	Ultimate torsion in pure torsion
α_{Col}	Parameter for evaluating the effectiveness of transverse reinforcement in resisting shear forces based on s/d ratio (ASCE SEI 41 − 17 (2017))
θ	Rotation
θ_p	Plastic rotation
θ_{pl}	Plastic rotation (rad) (ASCE SEI 41 − 17 (2017))
θ_y	Yield rotation
ρ_s	Transverse reinforcement ratio
Δ	Drift ratio
δ	Column top displacement
φ	Rebar diameter
φ_w	Stirrup diameter
φ_u	Ultimate curvature
φ_y	Yield curvature
μ	Ductility factor

1 Introduction

Countries located on active tectonic belts experience earthquakes that may cause both loss of life and property damage, directly threatening the safety of the building stock (Nascimbene 2024). It is crucial that existing buildings should be assessed with accurate methods

such that seismic risk can be mitigated. During seismic events, irregular buildings may experience torsional rotations that can strongly influence the behavior of members (Kamanli et al. 2023). As a result of torsion, reinforced concrete columns may experience loss of plastic rotation capacity, stiffness and ductility. These conditions can lead to the collapse of buildings earlier than estimated by using current assessment guidelines (TEC, ASCE, EC). Modern Performance-Based Earthquake Engineering (PBEE) frameworks heavily rely on accurate plastic rotation limits to assess structural damage states. Current guidelines do not include torsional effects while assessing deformation capacities of members. When evaluating the plastic rotation capacity of reinforced concrete columns, the effects of shear are taken into account. However, the stresses arising from torsion and those resulting from shear forces are fundamentally different from each other. Shear stresses in reinforced concrete columns are stresses that can cause inclined tensile failure by creating a unidirectional shear flow along the section height due to the effect of transverse forces; torsion stresses are shear stresses that occur due to the rotational effect around the longitudinal axis of the element and circulate in a closed loop around the section. Although both are types of shear stress, shear stresses are primarily countered by transverse reinforcement, whereas torsion stresses create circumferential tensile forces and therefore require the combined action of both transverse and longitudinal reinforcement, which is their fundamental difference.

Studies on the torsional behavior of reinforced concrete elements have been conducted since the early 19th century, particularly focusing on beams. The key aim of those studies was to design for torsion under the influence of torsion, shear and bending. Furthermore, the presence of axial load is known to significantly change the behavior of reinforced concrete elements. There are very few studies on the torsional behavior of reinforced concrete columns that simultaneously consider the effects of axial load, bending, and torsion. Since it is quite difficult to apply these three effects simultaneously in experimental studies, past research has generally attempted to understand the behavior under the action of axial load-bending, axial load-torsion, or bending-torsion.

The first systematic studies on torsion problems began in the late 18th century with Coulomb (1784) and were developed by scientists such as Navier (1826), Saint-Venant (1855), Bach (1890), and Timoshenko (1905) based on elasticity theory. However, the nonlinear and composite behavior of reinforced concrete led to the inadequacy of these theoretical approaches. The first significant step toward understanding the torsion behavior of reinforced concrete elements was taken by Rausch (1929) with the proposal of the "Space Truss Model". From the mid-20th century onwards, researchers such as Lessig (1959), Mitchell and Collins (1974), Hsu and Mo (1985), have demonstrated the limitations of elasticity theory through experimental studies and proposed advanced models such as the "Compression Field Theory (CFT)" and the "Softened Truss Model (STM)" to predict the torsional strength of reinforced concrete elements. These models provided more realistic results by considering the post-cracking behavior of concrete and material softening. The first comprehensive experimental studies on the torsional behavior of reinforced concrete columns began with Bishara and Peir (1968), followed by Hsu and Kemp (1969), Pandit and Mawal (1973), and Irani and Daniali (1993), who developed empirical formulas examining the interaction between axial load and torsion. Since the 2000s, cyclic tests have been conducted under more complex load combinations. Studies by Otsuka et al. (2004), Tirasit and Kawashima (2007), Belarbi et al. (2007), Nie et al. (2012), and Mullapudi and Ayoub (2013) systematically investigated the effects of parameters such as axial load ratio, torsional rota-

tion/drift ratio (θ/Δ), stirrup spacing, and section type on the ductility, energy dissipation, plastic hinge length, and ultimate strength of columns. Researchers have proposed empirical equations and interaction diagrams for modeling column behavior under combined loading. There are numerous experimental and analytical studies examining the behavior of reinforced concrete columns under combined effects such as axial load, bending, and torsion. In a pioneering study by Wang et al. (2014) on circular-section columns, it was observed that as the axial rotation/lateral displacement ratio increases, the plastic hinge length increases, while an increase in the bending effect reduces the rotation capacity. The study also found that the use of spiral transverse reinforcement leads to push-pull asymmetry, with longitudinal reinforcement improving bending resistance and transverse reinforcement improving torsional resistance. The researchers developed empirical equations modeling the behavior of circular-section columns under combined effects, similar to the approach proposed by Tirasit and Kawashima (2007) for square-section columns.

Deng et al. (2017) demonstrated that as the torsion-to-bending ratio increases in circular-section columns, the damage mechanism shifts from bending to torsion, and the plastic hinge length increases. While bending hysteresis loops become more robust, torsion loops rapidly narrow, and ductility values diverge. The study revealed that changes in column height and reinforcement ratios affect bending and torsional behavior to varying degrees. In studies covering different cross-sections and material types (Wang et al. 2018; Chen et al. 2018; He and Zhang 2020), it has been emphasized that the axial load level and cross-sectional geometry are decisive factors in torsional capacity and plastic hinge formation. In particular, Chen et al. (2018) defined three distinct failure modes based on the torsion-to-bending ratio and correlated them with the length of the plastic hinge.

Current research focuses on modeling column behavior under combined effects using more complex parameters and interaction diagrams. Attarchian et al. (2020) quantitatively demonstrated significant decreases in bending capacity and energy dissipation as the axial rotation/drift ratio increases; Cao et al. (2020) investigated the effect of axial load, concrete strength, and shear span ratio on torsional behavior in SRC columns, while Jiao et al. (2021) proposed new empirical equations for circular-section columns, while Yu and Shan (2021) presented an empirical equation and interaction diagram describing the pressure-bending-torsion interaction as a significant contribution to the literature. Zhou et al. (2022) found that dowels significantly improved the torsional performance of SRC columns, while Solak (2023) experimentally demonstrated the nonlinear effect of the axial load ratio on the torsional capacity and plastic hinge location in square-section columns. All these studies highlight the need to evaluate the torsional effect in conjunction with bending and axial loads for the realistic design of reinforced concrete columns.

Reinforced concrete structures built before the implementation of modern seismic design principles constitute a significant portion of the existing building stock, particularly in the Southern European basin; they contain critical structural defects such as the use of plain reinforcement, insufficient shear reinforcement, and deficiencies in detailing at beam-column connections. These deficiencies lead to the formation of brittle failure mechanisms and increased structural fragility under seismic loads. Experimental studies in the literature, particularly those conducted under the SPEAR project, have demonstrated that torsional effects resulting from plan irregularity are one of the most fundamental factors determining the seismic performance of such structures (Coehlo et al. 2005).

Torsional behavior arises from the eccentricity between the centers of mass and stiffness and leads to a strong coupling between the lateral displacement and rotation components under seismic loads (torsional coupling). In shake table tests, it was observed that high-stiffness columns and asymmetric balcony projections alter dynamic characteristics, causing excessive deformation concentrations in columns surrounding the structure. Rotations reaching their maximum values on upper floors can increase the structure's torsional sensitivity, potentially triggering the development of soft-story mechanisms.

Infill walls incorporated into the structural system, while initially enhancing structural stiffness and strength, further complicate torsional effects due to their asymmetric placements. During dynamic loading, damage to or sudden failure of infill walls leads to unpredictable shifts in the center of rigidity, intensifying the structure's dynamic response and torsional moments. Additionally, the additional shear forces generated in beam-column joint regions due to frame-wall interaction trigger the formation of shear hinges in these areas, thereby limiting the structure's ductility capacity (Pavese et al. 2017).

The use of recent multi-fidelity nonlinear fiber-based finite element models is critical for numerically predicting this complex behavior (Feng et al. 2024; Nascimbe 2015). Research confirms that accurately modeling the diaphragm effect of floor slabs and incorporating nonlinear capacities at connection zones into the analysis is essential for obtaining results consistent with experimental data. Particularly in structures where torsional effects are dominant, simplified models have been shown to be insufficient in capturing dynamic responses; conversely, advanced simulations that account for joint damage and infill wall interactions have been proven to provide more reliable predictions in seismic risk assessments.

A review of the literature reveals that as the torsion effect increases, the plastic hinge length of reinforced concrete columns tend to increase up to 1.5 times the section length (1.5 h). However no study has concentrated on examining the decrease in the rotation capacity of laterally loaded columns under combined effects of torsion and axial force.

The primary objective of this experimental study was to investigate the behavior of reinforced concrete columns subjected to axial load-bending-shear and torsion effects. The axial load ratio (n), rotation/drift ratio (θ/Δ), and stirrup spacing (s) are the key variables in this study. Based on the data obtained from the study, load-displacement, skeleton curve, stiffness, and energy dissipation graphs were obtained for the columns. The response of the tested columns was critically evaluated in terms of displacement ductility, plastic rotation capacity, interaction diagrams and plastic hinge lengths. Proposed plastic hinge length and the interaction model were compared with other models in the literature, and their effectiveness was discussed. The importance of the torsion effect was explained by comparing the plastic rotation values occurring in the columns with the plastic rotation limit values in TEC-2018 and ASCE/SEI 41 − 23. The outcomes of this work are believed to provide better estimation of reinforced concrete column response in buildings where torsional demands are significant.

This experimental study was designed to investigate the combined effects of axial load, bending, and torsion under laboratory conditions using cantilever column specimens. In actual structures, columns work in interaction with beams, slabs, and other structural system elements. However, in this experimental study, these interactions were neglected to allow for a clearer examination of local damage development, plastic hinge formation, and deformation capacity. Since the study investigated the effect of selected parameters on column behavior, it was considered that different structural interactions could alter these effects and

complicate the study's objective. The adopted θ/Δ ratios were intended to simulate torsional demands that may develop in columns due to seismic torsional irregularities. Although actual structural systems involve more complex boundary conditions and bidirectional seismic loading, the simplified setup allowed the isolated evaluation of torsion-related damage mechanisms and deformation capacities.

Numerous studies have examined the torsional behavior of reinforced concrete columns; however, experimental studies on the combined effects of axial load, bending, and torsion on the structural behavior of these columns are limited. In particular, previous studies have not sufficiently quantified the plastic rotation capacity and plastic hinge development of columns under torsion subjected to lateral cyclic loading. This study aims to address this gap by experimentally investigating the cyclic behavior of reinforced concrete columns under simultaneous axial load, bending, and torsion. This research is novel in that it (i) investigates the reduction in plastic rotation capacity under the combined effects of torsion and axial load, (ii) evaluates the effect of torsion on displacement ductility, energy distribution, and plastic hinge length, and (iii) proposes modifications to existing interaction and plastic hinge models based on experimental data. The plastic rotation capacities obtained from the tests were also compared with the limits specified in TEC-2018 and ASCE/SEI 41−23. The potential risks of neglecting the effects of torsion in the seismic performance assessment of reinforced concrete columns were highlighted.

2 Test methodology

2.1 Experiment design

Full scale square reinforced concrete specimens were prepared considering the typical dimensions, reinforcement, and other details of columns specified in the Turkish Building Seismic Code (TEC-2018) for mid-rise buildings. A total of 10 specimens were produced. The key parameters of the test specimens were axial load ratio ($n = N/f_c A_g$), stirrup spacing in the confined end (s) ratio of torsional angle of twist to drift ratio (θ/Δ). The test parameters of the specimens are presented in Table 1. It can be observed that the effect of axial load under the presence of torsion was studied by testing specimens T1-N10-S8, T1-N20-S8, T1-N30-S8, and T1-N40-S8. The effect of torsional deformation to drift ratio was investigated by testing specimens T0-N20-S8, T1-N20-S8, T2-N20-S8 and M0-20-S8. The effect of stirrup spacing was studied by testing specimens T1-N30-S8 and T1-N30-S16. Finally, the behavior of the specimens under pure torsion and in the absence of torsion (i.e. only lateral loading) was studied for two axial load levels by testing specimens T0-N20-S8, T0-N30-S8, M0-N20-S8 and M0-N30-S8.

Figure 1 presents the dimensions and reinforcement detailing of the test specimens. The dimensions of the column foundation were 1.2 × 1.0 × 0.5 m. The dimensions of the transverse beam above the column were 1.5 × 0.3 × 0.3 m. To prevent damage to the transverse beams during the experiment, longitudinal reinforcement of 10 14 mm diameter transverse reinforcement of 10 mm diameter with a spacing of 50 mm were used. Bending and torsion loads were applied to the column via the transverse beam. The distance between the two actuators on the beam was 1.2 m. The two actuators operated in tandem, applying different displacements to the ends of the transverse beam while imposing the prescribed lateral

Table 1 Details of test specimens

Specimen	θ/Δ	*n*	Concrete Strength (MPa)	Rebar Yielding Strength (MPa)	ρ_s	k_e	Stirrup (mm)
T1-N10-S8	1	0.10	24.24	400.36	0.0157	0.74	Φ10/80
T1-N20-S8	1	0.20	25.81	400.36			
T1-N30-S8	1	0.30	24.17	398.02			
T1-N40-S8	1	0.40	25.33	410.75			
T2-N20-S8	2	0.20	25.04	400.36			
T0-N20-S8	0	0.20	23.98	398.02			
T0-N30-S8	0	0.30	26.07	400.36			
M0-N20-S8	∞	0.20	26.32	410.75			
M0-N30-S8	∞	0.30	25.37	400.36			
T1-N30-S16	1	0.30	28.29	410.75	0.0078	0.49	Φ10/160

(θ: Rotation, Δ: Drift ratio, n: Axial load ratio, ρ_s: volumetric transverse reinforcement ratio, k_e: confinement effectiveness coefficient)

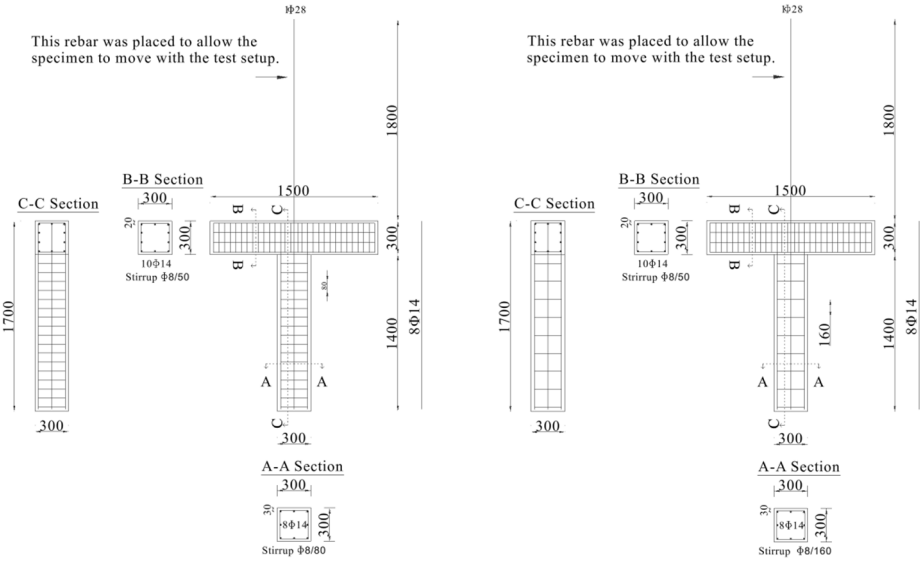

(a) (b)

Fig. 1 Rebar layout of specimens: (**a**) Stirrup spacing 80 mm; (**b**) Stirrup spacing 160 mm, with 8Ø14 mm longitudinal reinforcement bars

displacement and torsional rotations. The transverse beam was sufficiently reinforced, and no damage occurred during the experiment.

2.2 Materials and sizes of specimens

The specimens were produced using concrete with a 28-day cylinder compressive strength of 25 MPa. The modulus of elasticity (E_c) and tensile strength (f_t) were estimated using the empirical relations given in TS 500, based on the measured compressive strength, and were

calculated as E_c=30,250 MPa and f_t=1.75 MPa. Fracture energy was not directly measured in this study because the experimental program focused on the overall structural response rather than detailed material-level fracture modelling. For this reason, fracture energy was not used in the analysis. The mechanical properties of the reinforcing steel were determined through tensile tests. The yield, tensile, and ultimate strengths of the Ø8 reinforcement were 388.13 MPa, 465.67 MPa, and 448.93 MPa, respectively, while those of the Ø14 reinforcement were 403.04 MPa, 463.73 MPa, and 427.20 MPa. All specimens had a stirrup diameter of 10 mm and 8 longitudinal reinforcements with a diameter of 14 mm. The stirrup spacing was 80 mm in 9 specimens and 160 mm in 1 specimen. For all specimens, aspect ratio (b/h) is 1, the longitudinal reinforcement ratio (ρ_l) is 0.0136, the transverse reinforcement volumetric ratio (ρ_s) is 0.0094 for 80 mm spacing and 0.0047 for 160 mm spacing.

2.3 Loading protocols

In the experiments, a combined loading of axial load, bending, and torsion was applied to the columns. A 1000 kN capacity actuator was used for the axial load, whereas two 250 kN capacity actuators were used to impose lateral and torsional deformations.

The tests were conducted under displacement control according to ACI-374.1-13 (2013). Axial load was applied using a 1000 kN capacity actuator. This actuator operated in load control mode, and the load was kept constant throughout the test. Small fluctuations of ± 20 kN occurred due to cyclic lateral loading. However, these fluctuations did not significantly affect the test conditions. Second, lateral loads were applied according to the rotation/drift ratio (θ/Δ), and the test was continued until a 20% reduction in the lateral load capacity of the elements was observed. The tests were performed under reversed cyclic loading. An increase of 0.05% displacement ratio was provided at each loading step, and three fully reversed loading cycles were applied at each drift level (Fig. 2). Four different loadings were applied: pure bending (θ/Δ = 0), pure torsion (θ/Δ=∞), and two different combined bending-torsion loadings (θ/Δ = 1, θ/Δ = 2) (Fig. 3). Although the θ/Δ ratio used in this study does not directly represent the eccentricity of mass or stiffness in a structure, it is a normalized loading ratio commonly used in experimental parametric studies (Tirasit and Kawashima 2007). Further details can be found in Cengiz, 2025.

Two lateral actuators were controlled by applying separate displacements via a control panel. Each actuator was assigned a predetermined displacement increment via a separate control channel. To ensure coordinated movements of the actuators, they were synchronized with the automation system. The specimen underwent pure bending when equal displacements were assigned to both actuators. However, rotation occurred in the loading beam and torsional deformation occurred in the column when different displacements were applied.

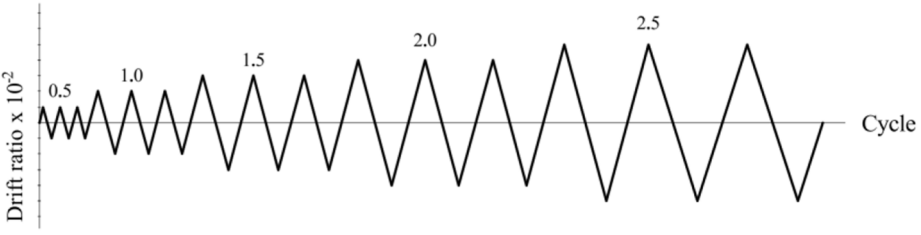

Fig. 2 Loading protocol (ACI-374.1-13 (2013))

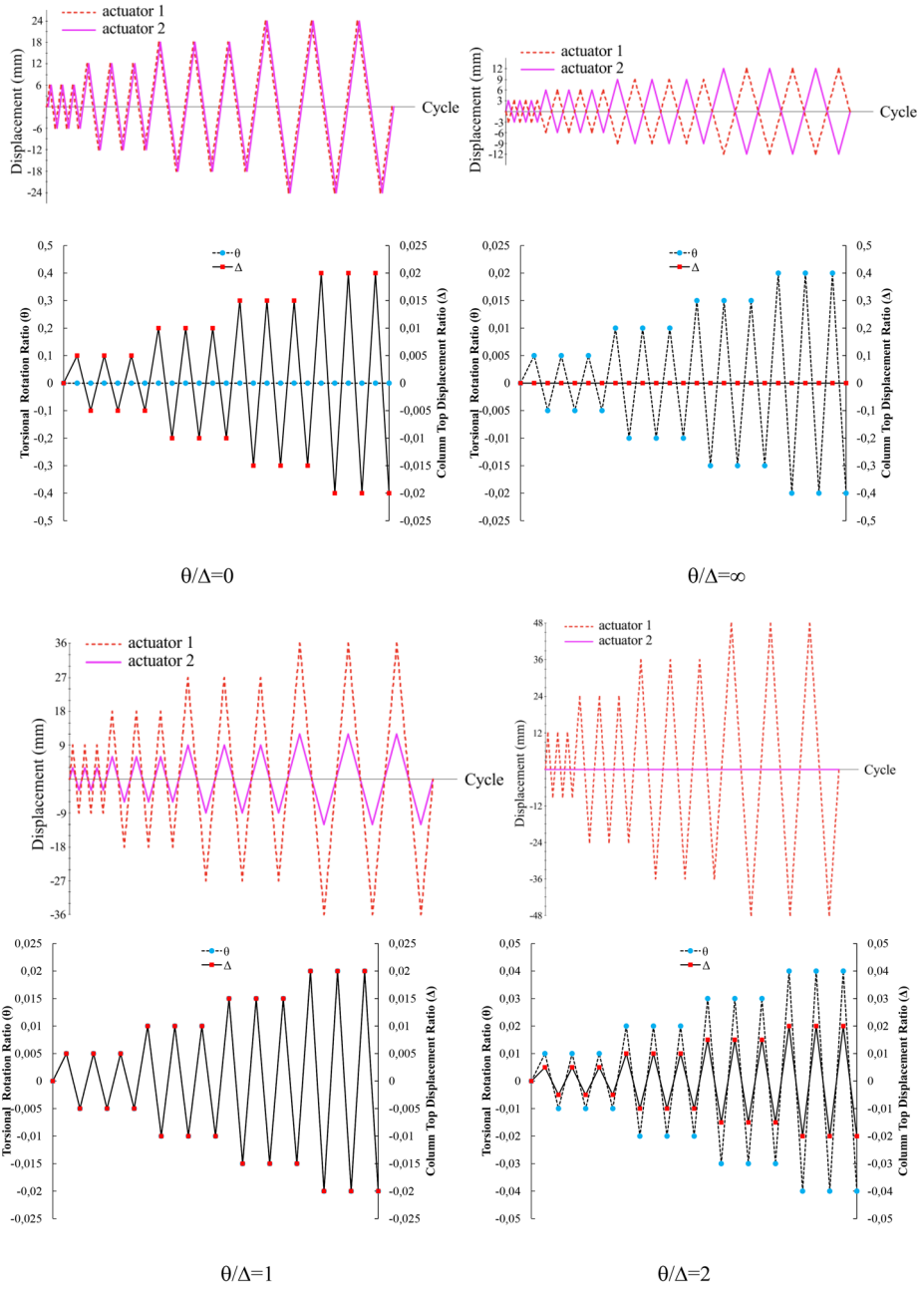

Fig. 3 Actuator displacement histories and prescribed torsional cyclic loading protocol for different θ/Δ ratios

The torsional rotation was controlled by a predetermined θ/Δ ratio, which allowed for the simultaneous application of bending and torsional loads during cyclic loading.

The two lateral actuators were controlled independently via separate hydraulic channels and operated simultaneously during the tests. By assigning different displacement amplitudes and loading rates to each actuator, both actuators reached their target displacements at the same time, thereby ensuring that the specified θ/Δ ratio was maintained throughout the cyclic loading protocol. Here, Δ is the column top displacement ratio calculated from Eq. (3), and θ is the rotation ratio calculated from Eq. (4). For specimens with $\theta/\Delta = 0$, equal displacement histories were applied to both actuators, resulting in pure bending without torsional rotation. For $\theta/\Delta = \infty$, equal but opposite displacements were applied, producing pure torsion without lateral displacement of the column's upper midpoint. For $\theta/\Delta = 1$ and $\theta/\Delta = 2$, different displacement amplitudes were applied to the actuators simultaneously, creating a combined bending-torsion loading in response to increasing torsional demand. Thus, bending and torsional actions were applied simultaneously and in-phase throughout the tests. Figure 3 presents the predicted torsional cyclic histories corresponding to each θ/Δ ratio, along with the actuator displacement histories.

The test setup is shown in Fig. 4. To apply the axial load, the steel loading beam (7) is fixed to the laboratory floor and connected to plastic hinges (12) on both sides. The actuator (9) that applies the axial load is hollow and cylindrical in shape. In Fig. 1, the 28 mm diameter reinforcement bar extending from the top of the column passes through the bearing (11), actuator (9), load cell (8), and loading beam (7), holding them all together. When torsion is applied to the specimens by applying different displacements to actuator 1 and actuator 2, the loading beam remains fixed and the elements can rotate around the axis thanks to the bearing.

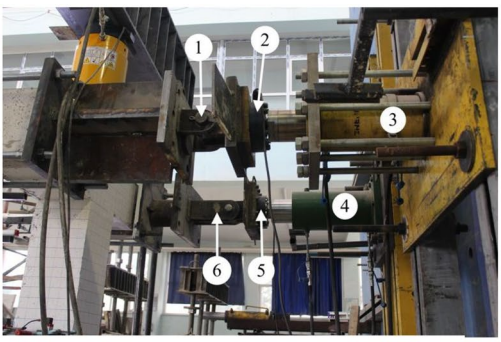

1: Hinge
2: Load-cell
3: Actuator1
4: Actuator2
5: Load-cell
6: Hinge
7: Loading beam
8: Load-cell
9: Actuator (axial load)
10: Actuator2
11: Roller bearing
12: Hinge
13: Footing (north side)

Fig. 4 Experimental setup

To ensure that the specimens behaved like cantilever columns, the foundation block was fixed to the laboratory floor using six high-strength bolts. LVDTs were placed on the top and lateral surfaces of the foundation block to record its displacement and rotation. However, due to the foundation block's high rigidity and its rigid fixation to the laboratory floor with high-strength bolts, no movement was observed in any of the specimens during the experiments.

The total lateral load (F) applied to the elements, the displacement amount at the element tip, the displacement ratio, the rotation angle, the bending moment M, and the torsion moment T are calculated as follows using the LVDT values shown in Fig. 5 (LC: Load-cell) (LVDT: Linear variable differential transformer):

$$\mathrm{F} = LC_{101} + LC_{103} \tag{1}$$

$$\delta = \frac{(\mathrm{LVDT}_{101} + \mathrm{LVDT}_{103})}{2} \tag{2}$$

$$\Delta = \frac{(\mathrm{LVDT}_{101} + \mathrm{LVDT}_{103})/2}{1200} \tag{3}$$

$$\theta = \frac{(\mathrm{LVDT}_{101} - \mathrm{LVDT}_{103})}{1200} \tag{4}$$

$$M = (LC_{101} + LC_{103}) \times 1{,}2 \tag{5}$$

$$T = (LC_{101} - LC_{103}) \times 1{,}2 \tag{6}$$

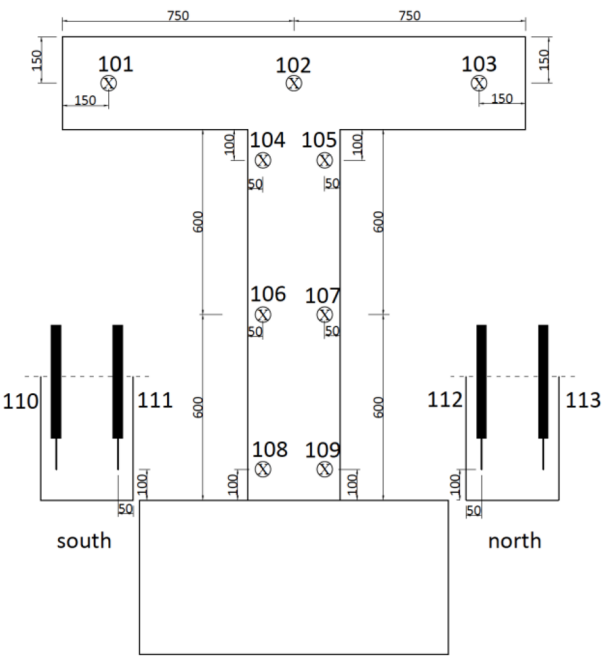

Fig. 5 LVDT locations on the specimens

Torsional rotation was calculated using the relative displacement difference between the end points of the loading beam, as given in Eq. 4. This expression provides the overall torsional rotation of the specimens and was used to verify the predicted θ/Δ ratios during the experiments. However, this approach does not account for irregular torsional distribution along the specimen height or conditions such as cross-sectional distortion. Since the specimens were tested as a rigid transverse loading beam and short cantilever columns with square cross-sections, it was assumed that the torsional behavior was primarily governed by uniform Saint-Venant-type torsion. Therefore, the torsional behavior should be interpreted as the specimen's overall torsional behavior rather than a detailed representation of the local torsional strain distribution.

3 Evaluation and discussion of test results

The measured load-deflection responses of the test specimens are presented in Fig. 6. The pictures of the damaged specimens and the crack and damage maps of the specimens are shown in Figs. 7 and 8. The summary of the test results in terms of lateral load carrying capacity, measured crack widths at 2%, plastic hinge lengths, displacement ductilities and cumulative dissipated energies are presented in Table 2. First cracks in the T1 specimens were observed at a drift ratio of 0.5%. Initial cracks with widths of approximately 0.3 mm formed as flexural and inclined torsional cracks along the column. The lateral load carrying capacity was observed around 2.0% interstory drift ratio with maximum flexural and shear crack widths of about 1.5 and 1.0 mm, respectively. At a drift ratio of 2.5%, the concrete cover began to spal. Although there was no bar buckling of the T1-N10-S8, bar buckling occurred in the T1-N20-S8, T1-N30-S8, and T1-N40-S8. With the stirrup spacing increased to 160 mm in T1-N30-S16, plastic hinges formed throughout the entire height of the specimen. The specimen failed in a premature and sudden manner at about 2% drift ratio caused by rebar buckling.

For specimens with θ/Δ ratio was 2 (T2-N20-S8), a torsion dominated response was observed, and the initial cracks appeared as inclined cracks of approximately 0.3 mm, indicating increased shear demand. The lateral load increased up to a drift ratio of 1.5% before dropping abruptly. Although direct shear strain or diagonal compression measurements were not performed in the experimental study, the observed crack patterns and fracture shapes indicate that the torsion effect contributed to the formation of additional shear stresses in the specimens. The experiment continued up to a 2.0% drift ratio. The plastic hinge length formed at the end of the experiment was 600 mm. Buckling was observed in the longitudinal reinforcements.

T0-type specimens subjected to pure bending with $\theta/\Delta=0$ exhibited flexural dominated response as expected. In both specimens, cracks formed as bending cracks 0.3 mm width during the first cycle. No shear cracks formed throughout the test. The tests were continued up to a drift ratio of 5.5%. The plastic hinge length was 150 mm in the T0-N20-S8 and 200 mm in the T0-N30-S8. No buckling occurred in the longitudinal reinforcement in both specimens due to relatively closed tie spacing.

M0-type specimens subjected to pure torsion with $\theta/\Delta=\infty$ had torsion cracks forming completely along the height of the specimens. The tests on both specimens were continued up to 0.055 rad of rotation. Bar buckling was not observed in the longitudinal reinforce-

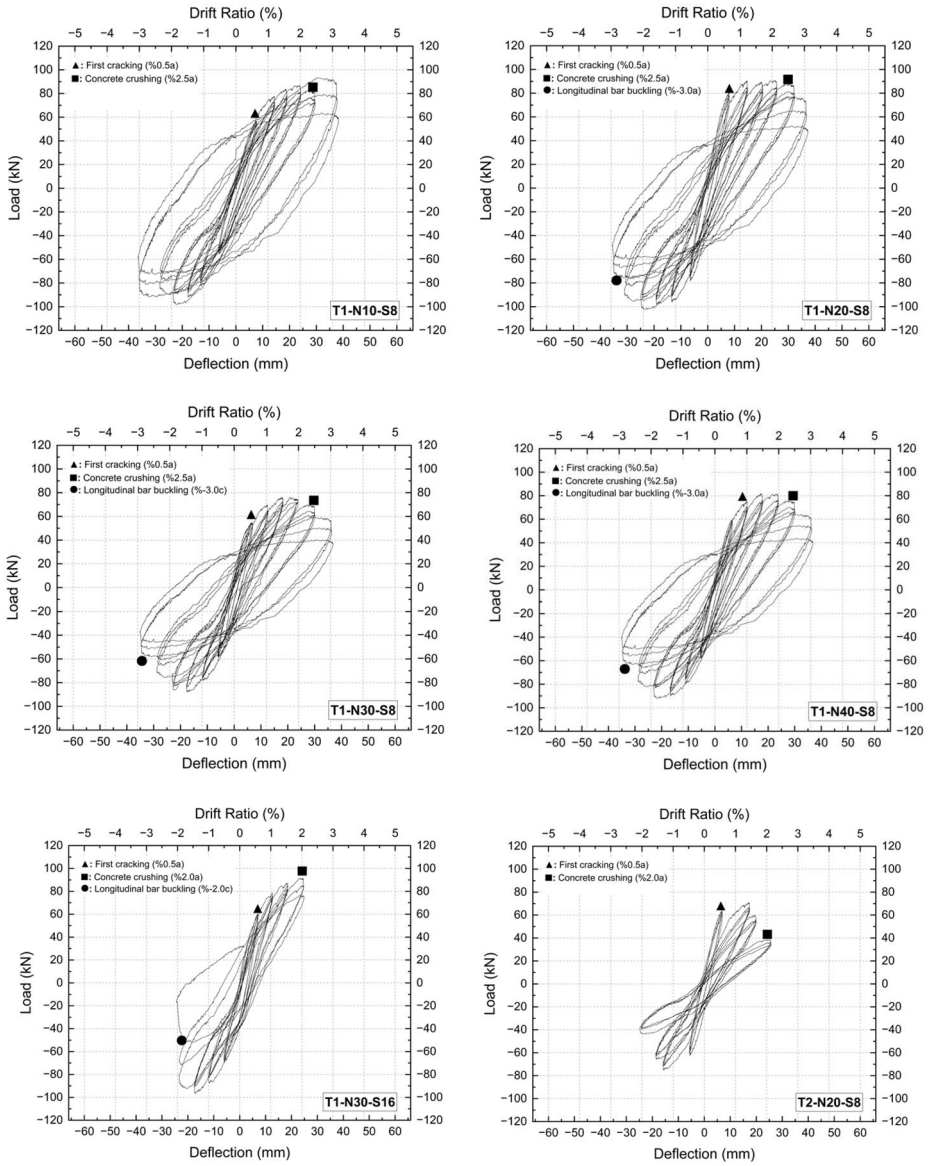

Fig. 6 Hysteresis curves of specimens

ments of the M0-N20-S8, but it did occur in the M0-N30-S8. The plastic hinge region in the M0-N20-S8 formed near the bottom end of the column, while that of the M0-N30-S8 formed at the top end of the column.

Results showed that the presence of torsion directly affected the plastic hinge length formed in the specimens. In T0 type specimens without torsion, a plastic hinge length of approximately 0.5 h was formed, as reported in the literature (TEC-2018). Theoretical plastic hinge lengths are also shown in Table 3. Since the loading was in the east-west direction,

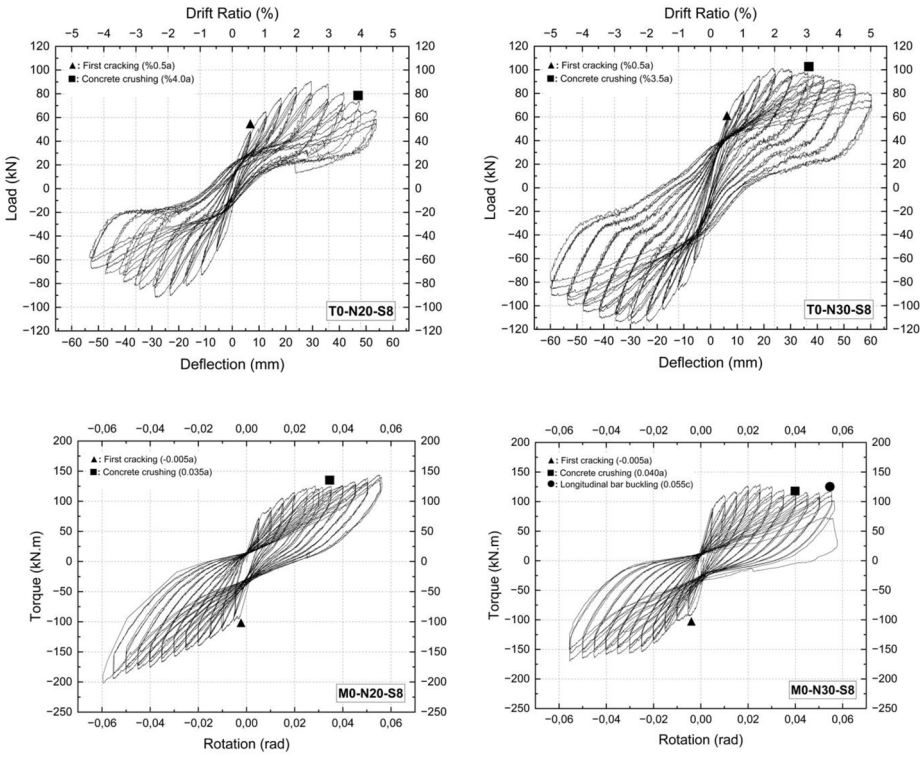

Figure 6 (continued)

the damage occurred mainly on the specimen faces in this direction and was concentrated at the corners.

3.1 Effect of axial load

The behavior of the specimens T1-N10-S8, T1-N20-S8, T1-N30-S8, and T1-N40-S8 were compared to study the influence of axial loads for specimens with torsion. Experimental data showed that axial load significantly affected the column behavior under combined bending-torsion loading. When load-carrying capacities are compared using the T1-N10-S8 as a reference, T1-N20-S8 had a slightly higher load-carrying capacity, T1-N30-S8 and T1-N40-S8 had approximately 10–15% lower lateral load-carrying capacities (Fig. 9a). Similar behavior was observed in stiffness and energy dissipation values. The energy dissipation value of the T1-N20-S8 was the highest, while that of the T1-N30-S8 was the lowest (Fig. 9b and c). Longitudinal reinforcement buckling occurred in all specimens except the T1-N10-S8. As the axial load increased, the number of cracks reduced, crack widths increased, and cracks formed at a steeper angle. The drift capacity of the specimens under consideration was significantly reduced as a function of axial load. For the lowest axial load ratio of 0.1, the drift capacity defined as the drift ratio at 20% reduction of lateral load was about 3% whereas it was about 2% for the specimen with the axial load ratio of 0.4. This behavior aligns well with established concrete confinement theories. At higher axial load levels, the concrete

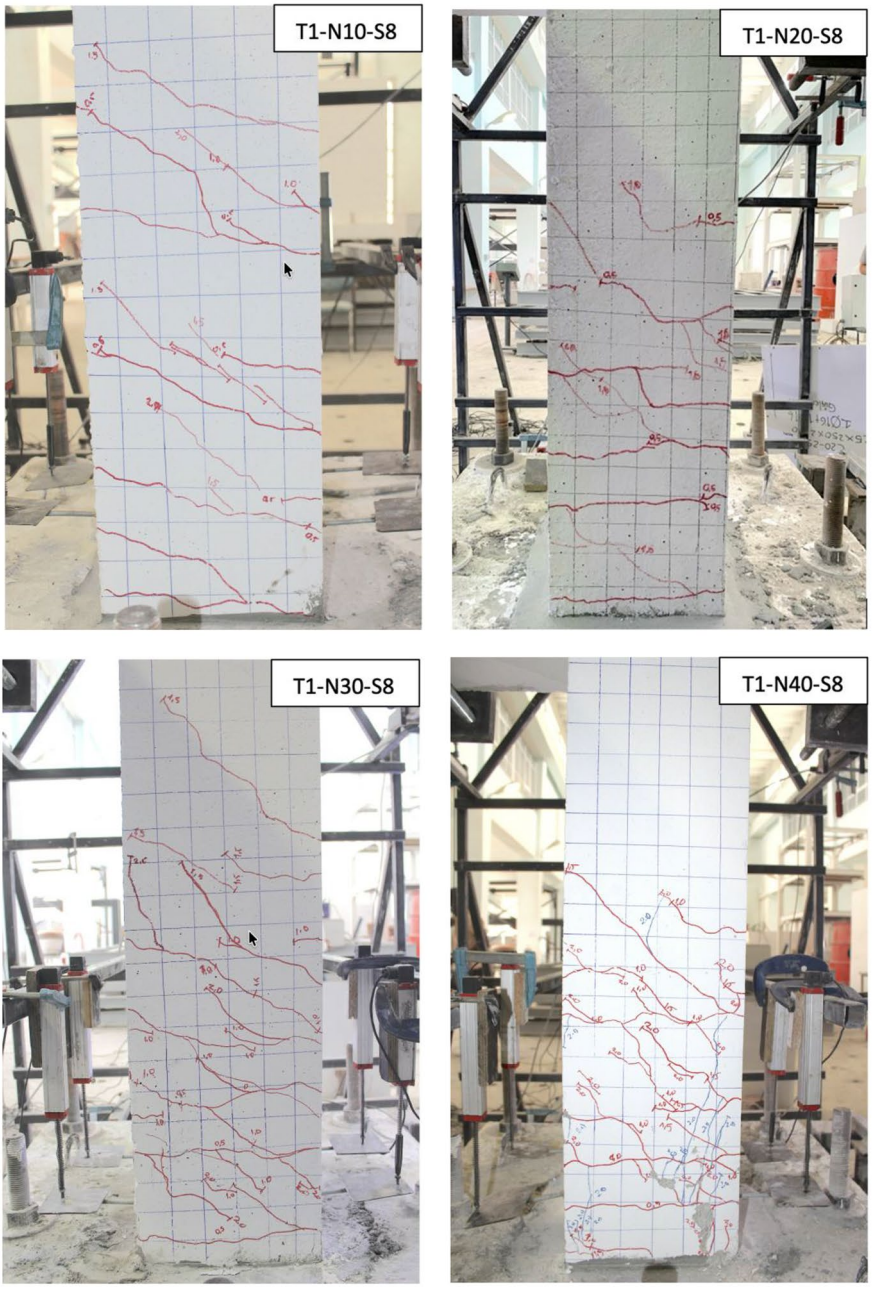

Fig. 7 Cracks on specimens at 2.0% drift ratio (west side) (for M0 type specimens at 0.030 rad) (Each square drawn on the elements measures 50 × 50 mm.)

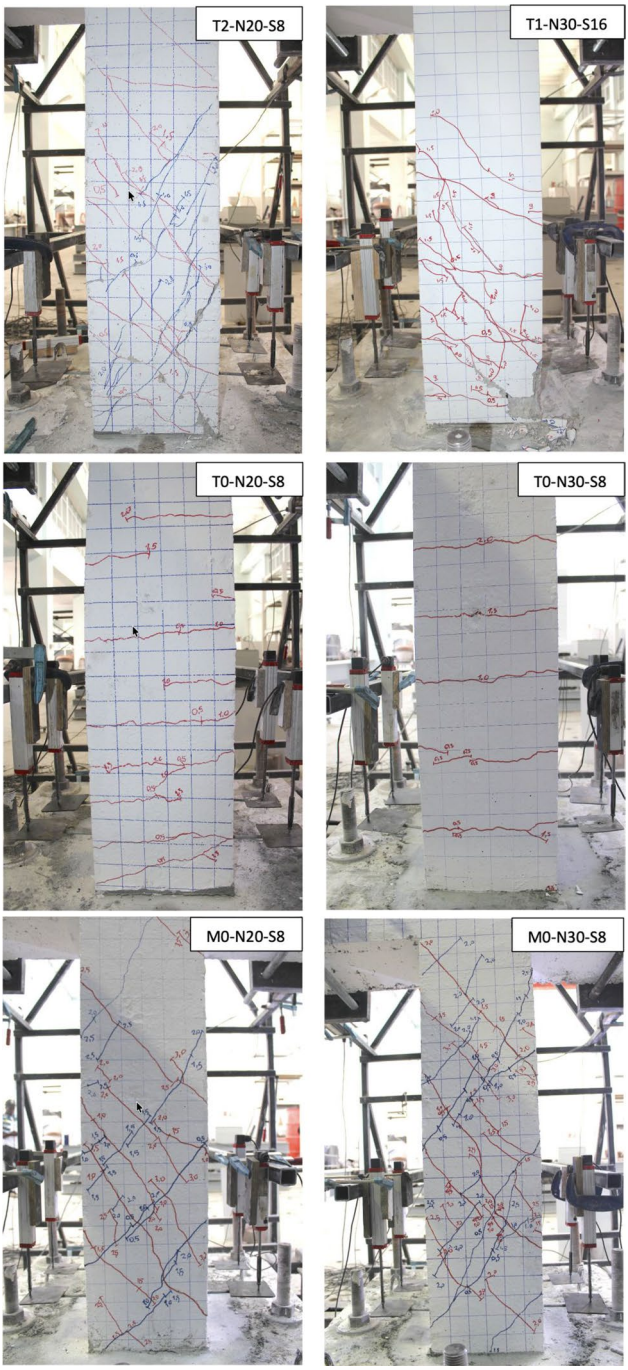

Figure 7 (continued)

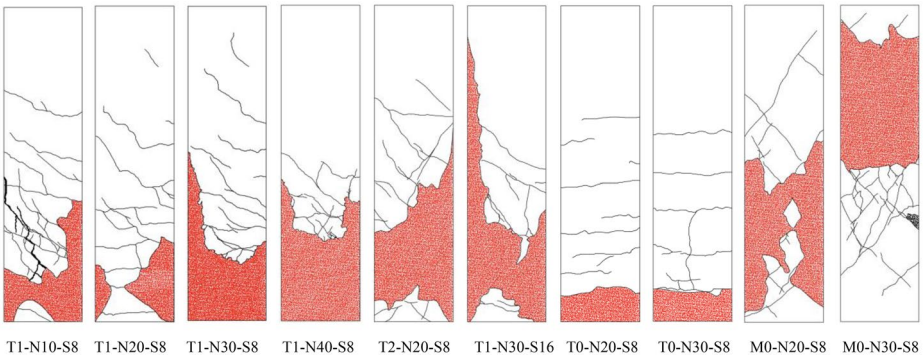

Fig. 8 Crack maps of the specimens (west side)

experiences excessive compressive stresses that rapidly exhaust the confinement capacity of the stirrups. This leads to premature concrete crushing, early yielding of the transverse reinforcement, and subsequent longitudinal bar buckling, which fundamentally restricts the member's ductility and rotational capacity (Mander et al. 1988).

3.2 Effect of torsion

To investigate the effect of torsion on the behavior of the specimens, the T0-N20-S8, T1-N20-S8, and T2-N20-S8 were compared. The results obtained from the experimental data showed that torsion changed the behavior of the specimens. Although the load-carrying capacities of the T0-N20-S8 and T1-N20-S8 are almost the same, the load carrying capacity of the T2-N20-S8 is 22% lower. The presence of torsion significantly reduced the displacement capacities of the specimens. In the absence of torsion, the T0-N20-S8 sustained its load carrying capacity up to a drift ratio of 4.5%, this value was 3% and 2% for T1-N20-S8 and T2-N20-S8 up to 2.0% (Fig. 10a). An increase in torsional demand likely leads to the development of additional shear stresses in the specimens, thereby reducing their deformation capacity under bending.

In this study, although the observed crack patterns, damage concentration, and hysteretic response indicate significant shear-torsion interaction in the tested specimens, direct measurements of shear stress, diagonal compression, or internal stress redistribution were not performed in the experimental program. Therefore, the identification of failure mechanisms in this study is based on the observed crack propagation, damage distribution, and overall structural response. Accordingly, the results regarding the shear-torsion interaction should be interpreted as observational.

Consequently, shear-related damage was observed to spread across the specimen surface and is interpreted to have contributed to the ultimate state. This resulted in reduced stiffness and energy dissipation capacity (Fig. 10b and c). The highest energy dissipation occurred in T1-N20-S8, while the lowest energy dissipation occurred in T2-N20-S8. Comparing the cumulative energy dissipation values with the T0-N20-S8 as a reference, T1-N20-S8 had 115% and T2-N20-S8 had 28% energy dissipation capacity. When the θ/Δ ratio is compared between 0 and 1, a 15% difference in energy dissipation capacity is observed, while when this ratio increased to 2, i.e., when torsion increases, the energy dissipation capacity is seen

Table 2 Results of the experiments

Specimen	Lateral Load Capacity (kN) Push/Pull	Crack Width at 2% Drift Ratio (mm) Bending/Shear	Plastic Hinge Length (mm)	Yield Displacement (mm)		Ultimate Displacement (mm)		Cumulative Energy Dissipation Capacity (kN.m)
				Push	Pull	Push	Pull	
T1-N10-S8	86.11/-96.55	1.6/1.1	500	13.1	-12.0	36.0	-36.0	12.29
T1-N20-S8	89.95/-101.85	3.5/0.8	350	9.1	-8.1	36.0	-35.2	12.38
T1-N30-S8	75.05/-87.98	1.4/0.6	600	9.5	-9.5	36.0	-35.1	9.31
T1-N40-S8	81.58/-90.53	1.5/0.8	550	9.7	-10.1	36.0	-35.1	9.94
T2-N20-S8	70.41/-74.49	1.2/2.8	750	8.2	-7.0	21.5	-21.0	2.93
T1-N30-S16	90.07/-96.42	Crack width>5*	1200	11.3	-8.1	24.0	-23.2	3.85
T0-N20-S8	89.98/-91.69	1.4/0	150	10.5	-10.8	48.0	-47.5	11.73
T0-N30-S8	100.36/-113.81	0.9/0	200	10.9	-11.1	59.1	-59.0	25.54

* The specimen failed prematurely and suddenly at this drift ratio

Table 3 Comparison of experimental and theoretical models

Specimen	*Experimental L_p	*Theoretical L_p Eq. 12	Priestley and Park (1987)	Priestley et al. (1996)	Tirasit and Kawashima (2007)	Berry and Eberhard (2008)	Bae and Bayrak (2008)
T1-N10-S8	500	490	180	153	202	174	73
T1-N20-S8	350	345	180	153	202	170	75
T1-N30-S8	600	595	180	153	202	173	77
T1-N40-S8	550	540	180	153	202	174	80
T2-N20-S8	750	740	180	153	241	171	75
T1-N30-S16	1200	1210	180	153	202	168	77
T0-N20-S8	150	150	180	153	150	174	75
T0-N30-S8	200	195	180	153	150	170	77

Note: All dimension is mm. *Average difference between Experimental and Theoretical L_p: 1.3% Linear regression was performed, and the coefficient of determination (R^2) was calculated as 0.999678

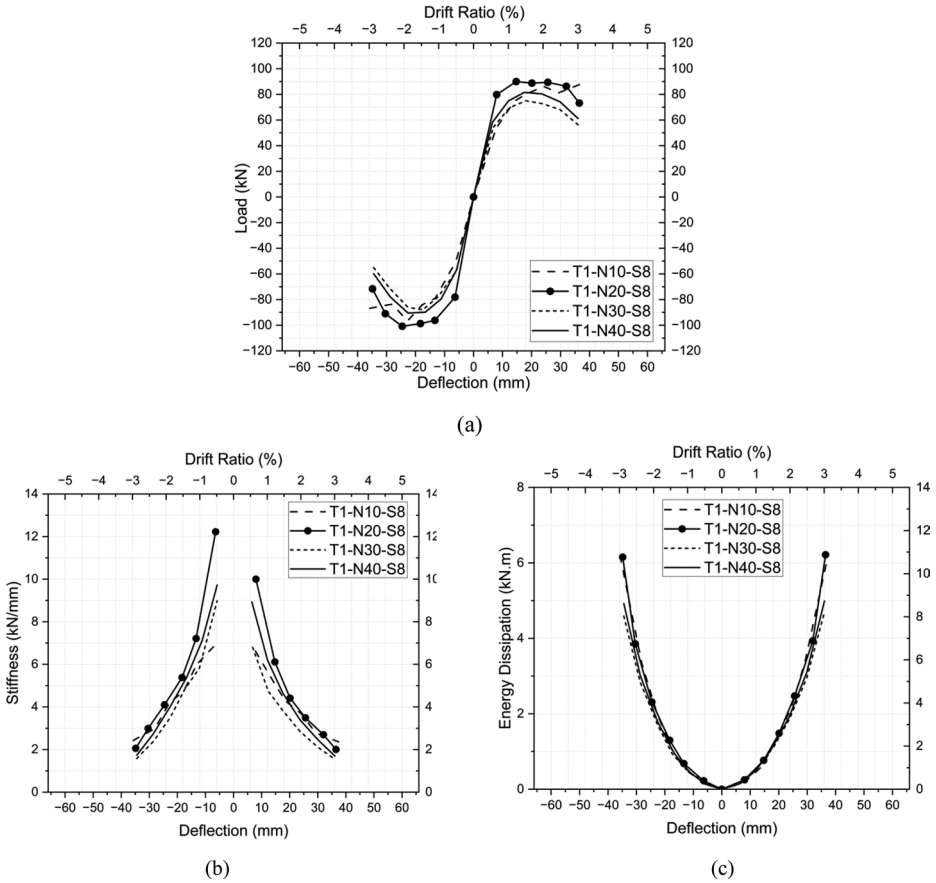

Fig. 9 Effect of the axial load: (**a**) backbone curves; (**b**) stiffness; (**c**) energy dissipation

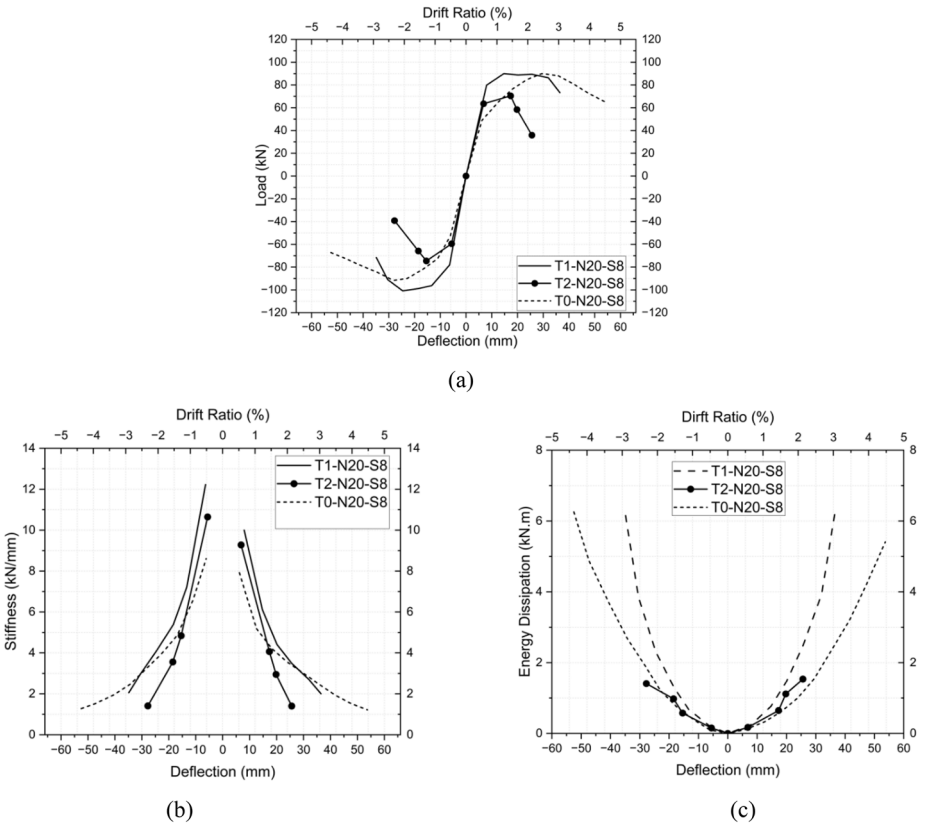

Fig. 10 Effect of the torsion: (**a**) backbone curves; (**b**) stiffness; (**c**) energy dissipation

to decrease by 62%. When the θ/Δ ratio increased from 0 to 1, the flexural crack width increased by 2.5 times. Inclined cracks associated with increased torsional demand were observed, suggesting additional shear-related damage. When the θ/Δ ratio increased from 1 to 2, the flexural crack width decreased by 0.34 times, while the shear crack width increased by 3.5 times. The crack angles formed in the T0-N20-S8, T1-N20-S8, and T2-N20-S8 are 0°, 15°-45°, and 45°-60°, respectively.

3.3 Effect of stirrup spacing

To investigate the effect of the stirrup spacing on the behavior of the specimens, the T1-N30-S8 and T1-N30-S16 were compared. The T1-N30-S16 carried 20% more load than the T1-N30-S8 but exhibited 33% less displacement (push direction) (Fig. 11a). The stirrups in both members subjected to bending-torsion loads counteracted the shear stresses developed in the members. The crack patterns and damage progression in the T1-N30-S16 member, with a stirrup spacing of 160 mm, mobilized a larger portion of their capacity and continued to bear the load until plastic deformation occurred. When the stirrups in the T1-N30-S16 member approached their stress–strain capacity, significant damage localiza-

tion was observed, which is interpreted to have contributed to the abrupt failure of the specimen. In the T1-N30-S8 element, which has a stirrup spacing of 80 mm, the shear stresses were countered by a greater number of stirrups; consequently, the stirrups remained within the yield stress range, and no failure occurred. This situation caused the bending capacity of the T1-N30-S8 to be lower than that of the T1-N30-S16 because the stirrups did not extend into the hardening zone. When the stirrup spacing increased to 160 mm, the initial stiffness decreased by 12% and the energy dissipation capacity decreased by 57% (Fig. 11b and c). At a drift ratio of 0.2%, the shear crack width was 1.6 mm in the T1-N30-S8, while it was more than 5.0 mm in the T1-N30-S16. Longitudinal reinforcement buckling occurred in both specimens. Damage occurred at the edges of the T1-N30-S8, while all damage in the T1-N30-S6 occurred at the corners.

3.4 Plastic hinge length

The plastic hinge length mentioned in the specimens is based on observations of the damage distribution occurring in the specimens. The region characterized by intense cracking and

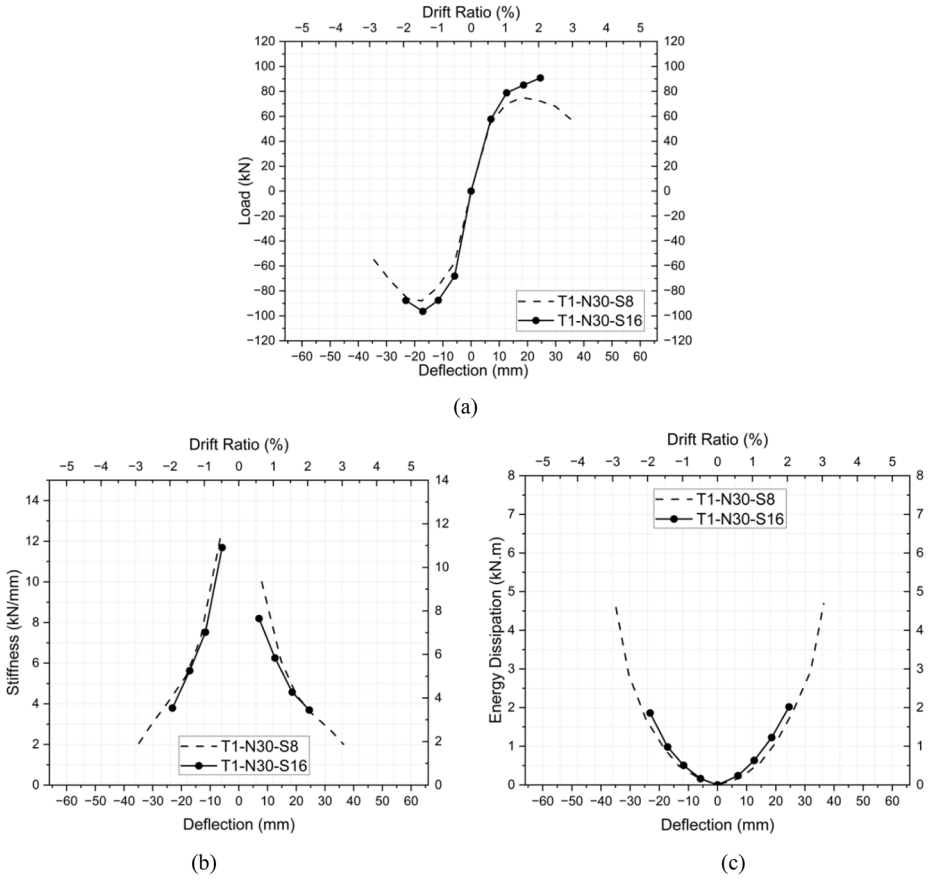

Fig. 11 Effect of the stirrup spacing: (**a**) backbone curves; (**b**) stiffness; (**c**) energy dissipation

concrete spalling in the specimens is defined as the plastic hinge region, and the height of this region from the column base is defined as the plastic hinge length.

The plastic hinge length formed in the specimens was found to be directly related to the loading type. In T0-type specimens subjected to pure bending, the plastic hinge length formed was approximately 0.5 h and increased with axial load. The experimental observations indicate that the presence of torsion was associated with an increase in plastic hinge length of approximately 400%. In addition, a nonlinear relationship was observed between the axial load and the plastic hinge length. Moderate axial loads initially cause the plastic zone to spread over a wider area. However, once a critical axial load threshold is exceeded, this trend reverses. High axial load combined with torsion accelerated concrete deterioration. As a result, the plastic hinge region became shorter, which limited the overall ductility capacity of the specimens. The parameter that also affected the plastic hinge length was the stirrup spacing. A plastic hinge was observed along the height of T1-N30-S16 where it was about 600 mm for the companion specimen with lower torsional demand (T1-N30-S8). The plastic hinge length (350 mm) occurred in the T1-N20-S8 was significantly less than the plastic hinge length occurred in other T1 type specimens.

The plastic hinge length (L_p) is a critical parameter in evaluating the seismic performance of reinforced concrete columns. There are a number of different proposals for the plastic hinge length in the literature.

Priestley and Park (1987 (Eq. 7) were the first to demonstrate that the longitudinal reinforcement diameter affects the plastic hinge length of reinforced concrete columns. However, since this model did not include any load effects, it remained quite simple. Priestley et al. (1996) considered both the reinforcement diameter and the yield strength of the reinforcement (Eq. 8). Until 2007, most studies on plastic hinge length focused on improving the coefficients in existing models. Later, Tirasit and Kawashima (2007) investigated how different bending and torsion effects change the plastic hinge length formed in reinforced concrete columns. The authors introduced a new plastic hinge model using the bending-torsion interaction, bringing a highly innovative approach to this subject (Eq. 9). However, one of the major problems with this model was the neglect of the axial load effect. Berry and Eberhard (2008) presented a new model considering the reinforcement diameter, reinforcement yield strength, and concrete compressive strength (Eq. 10). However, this model does not include any parameters related to external loads. Bae and Bayrak (2008) filled an important gap in the literature by including the axial load effect (Eq. 11). Among these models only that of Tirasit and Kawashima included the effect of torsion. In Eq. 9, which takes the torsion effect into account, the plastic hinge length can take values up to 1.5D, while in other models it can reach a maximum value of 0.5D. Therefore, it can be seen that in models that do not take the torsion effect into account, the plastic hinge length calculation will yield incorrect results. The comparison of the plastic hinge length predictions with all the models are presented in Table 3. Experimental results demonstrated that test results significantly differ from the observed plastic hinge lengths from the tests under consideration.

$$L_p = 0.08L + 6d_b \tag{7}$$

$$L_p = 0.08h + 0.022d_b f_y \tag{8}$$

$$L_p = 0.5D(r+1)^{0.43} \leq 1.5D \tag{9}$$

$$L_p = 0.05L + 0.1d_b \frac{f_y}{\sqrt{f'_c}} \tag{10}$$

$$\frac{L_p}{h} = \left[0.3\left(\frac{P}{P_0}\right) + 3\left(\frac{A_s}{A_g}\right) - 0.1\right]\left(\frac{L}{h}\right) + 0.25 \geq 0.25 \tag{11}$$

In order to improve the ability of estimating the plastic hinge length, plastic hinge lengths obtained from this study conducted under different axial load ratios (n), rotation/drift ratio ($r=\theta/\Delta$), and stirrup spacings (s) are analyzed, and an empirical prediction model is developed. Since L_p and h have the same unit (mm), the L_p/h ratio, s/h ratio, r, and n parameters are dimensionless. Therefore, the model is dimensionally consistent and does not require additional dimensional analysis. The model form was determined to best fit the experimental data, as is the case with many empirical models in the literature. Using dimensionless analysis and multiple regression methods, the following empirical equation has been derived (Eq. 11):

$$L_p = 0.7h(1 + 1.5 \cdot r)(1 + 2 \cdot n)\left(\frac{s}{h}\right)^{0.8} \tag{12}$$

Above, r is the rotation/drift ratio, n is the axial load ratio, s is the stirrup spacing (80–160 mm), and h is the column cross section (300 mm). The model coefficients were determined using nonlinear least-squares regression. The model form was chosen as a multiplicative combination of independent parameters, each representing a different physical effect; the exponents and coefficients were iteratively adjusted to provide the best fit to the experimental data while preserving physically meaningful trends. The proposed model exhibits an average error of 1.3% compared to the experimental values, and the random distribution of the residuals around zero indicates the absence of systematic bias.

The empirical model proposed in Eq. 12 was derived from the experimental dataset obtained in this study. Despite the limited number of specimens, the model reasonably represents the observed trends in plastic hinge length according to the axial load ratio, torsional demand, and stirrup spacing. The experimental results indicate that torsion increases L_p. The distribution of experimental and theoretical values (R^2 = 0.999678) indicates that Eq. (12) is applicable for the range of tested parameters. Furthermore, including the (s/h) parameter in the proposed equation reflects the observed trend in the test results rather than establishing a generalized statistical relationship. Due to the limited dataset used in this study, the coefficient of determination was found to be relatively large. It should be noted that changes in specimen properties and applied loads may cause the coefficient of determination to decrease.

The experimental results are compared with the developed model in Table 3. A good agreement is observed between the results of the equation and the test results (Fig. 12). It should be noted that the estimated plastic hinge length using Eq. 12 in the absence of torsion varies between 0.5 h and 0.7 h when n values vary between 0.1 and 0.4 for s equals to h/2. When r value increases to 1, the expected damage zone denoted as the plastic hinge length increased by up to 2.5 times that of these values. The proposed empirical model was calibrated with eight experimental data points. Due to the limited number of data points, this study is a preliminary investigation examining the effect of torsion on plastic hinge length.

3.5 Interaction model

There a number of interaction models including bending, shear, torsion and axial load on reinforced concrete columns (Ersoy and Ferguson 1968; Ewida and McMullen 1981; Hsu and Mo 2010; Yu and Shan 2021). The models are summarized in Table 4. Among these models, interaction equation of Yuan and Shan (2021) hereafter referred to as the YS Model, is the only one incorporating all relevant variables, i.e., axial force, shear force, bending moment and torsion. The model shows that axial compression at a certain level ($N/N_0 \leq 0.25$) increases the bending capacity (negative term), but shear and torsion reduce the carrying capacity with quadratic effects. It is emphasized that $T/T_0 = 0.62$ is the critical threshold for torsion damage. Unlike the literature, this model, which considers four load types together, allows for a more realistic assessment of load interactions in the design of complex structures such as curved bridge beams. However, it is recommended that the model be extended for different sections, concrete classes and loading scenarios.

The YS Model provides an important contribution to defining the relationship between axial load, bending moment, shear force, and torsional moment. However, the expression of the axial load term with a negative coefficient (-3.12) in the model necessitates some math-

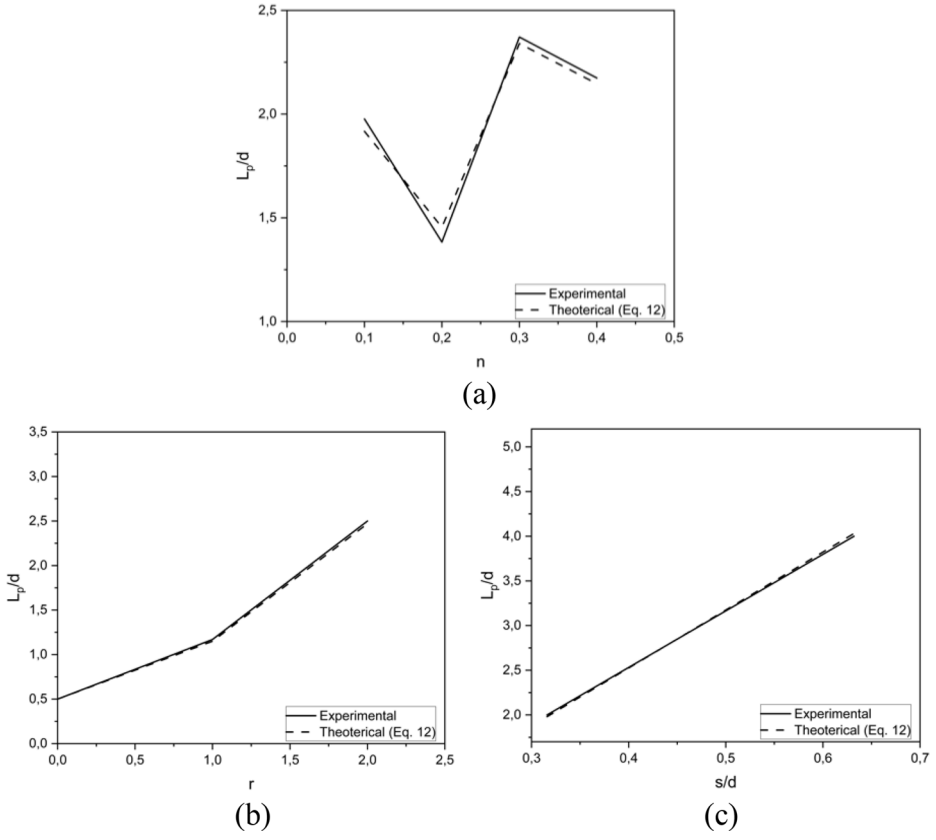

Fig. 12 Comparison of the plastic hinge length obtained from the proposed formula and the experiment: (**a**) axial load effect; (**b**) torque effect; (**c**) stirrup effect

Table 4 Interaction models

Research	Model	Loading Type
Ersoy and Ferguson (1968)	$\left(\frac{T}{T_0}\right)^2+\left(\frac{V}{V_0}\right)^2=1$	V-T
Ewida and McMullen (1981)	$\left(\frac{T_u}{T_{u0}}\right)^2+\left(\frac{V_u}{V_{u0}}\right)^2+\left(\frac{M_u}{M_{u0}}\right)=1$	M-V-T
Hsu and Mo (2010)	$\left(\frac{M}{M_0}\right)+\left(\frac{V}{V_0}\right)^2R+\left(\frac{T}{T_0}\right)^2R=1$ $-\left(\frac{M}{M_0}\right)\frac{1}{R}+\left(\frac{V}{V_0}\right)^2+\left(\frac{T}{T_0}\right)^2=1$ $\left(\frac{V}{V_0}\right)^2+\left(\frac{T}{T_0}\right)^2+\sqrt{2}\left(\frac{VT}{V_0T_0}\right)=\frac{1+R}{2R}$	M-V-T
Yu and Shan (2021)	$-3.12\left(\frac{N}{N_0}\right)+1.01\left(\frac{M}{M_0}\right)^2+1.35\left(\frac{V}{V_0}\right)^2+1.01\left(\frac{T}{T_0}\right)^2=1$	N-M-V-T

ematical and physical evaluations. The negative coefficient causes an increase in the axial load ratio to decrease the left side of the equation, which may lead to different approaches in interpreting the effect of axial load on capacity. Furthermore, comparative calculations performed on the same data set indicate that some discrepancies may be observed in the agreement between the YS Model and experimental results, particularly in cases where shear force data is unavailable, suggesting that the applicability of the model may be limited.

Based on the data obtained from this study, a new interaction model that simultaneously incorporates Axial Load–Bending–Torsion (N-M-T) effects is presented (Eq. 13). The interaction relationship proposed in this equation is an empirical formulation derived from results obtained from specimens tested within the scope of this study. When creating the model, the torsional moment capacity (T), bending moment capacity (M), torsional strength under simple torsion (T_0), and bending strength under simple bending (M_0) values for each specimen were taken into account. The ratios T/T_0 and M/M_0 were calculated to ensure that the interaction model was dimensionless. The exponential expressions in this model were determined using regression analysis to best capture the interaction between axial load, bending moment, and torsional moment obtained from experiments. In the proposed model, the shear effect has been neglected because the shear cannot be precisely determined due to asymmetric loading in the elements. The relevant data for the specimens are shown in Table 5.

$$\left(\frac{N}{N_0}\right)^{1.2}+\left(\frac{M}{M_0}\right)^{1.5}+\left(\frac{T}{T_0}\right)^{1.8}=1 \tag{13}$$

In the model proposed in this study (Eq. 13), all parameters are expressed with positive coefficients, and the exponential values (1.2 for axial load, 1.5 for bending, and 1.8 for torsion) have been determined in line with similar studies in the literature. The model achieved a high level of agreement with an average error rate of 2.2% as a result of calibration performed with experimental data. All terms' coefficients have been set to 1, thus ensuring dimensional consistency.

In this study, while developing the interaction model proposed in Eq. 13, different axial load, bending, and torsion effects were considered. The most significant difference between this model and the Yu and Shan (2021) model expressed in the cross-section property. While

Table 5 Data used for the interaction model

Specimen	Loading Type	Torsional Capacity (T) (kN.m)	Bending Capacity (M) (kN.m)	T/T_0	M/M_0
T1-N10-S8	Bending-Torsion	97.74	103.54	1.85	0.94
T1-N20-S8	Bending-Torsion	103.47	107.94	1.96	0.98
T1-N30-S8	Bending-Torsion	120.80	90.06	2.29	0.82
T1-N40-S8	Bending-Torsion	135.43	96.42	2.57	0.87
T2-N20-S8	Bending-Torsion	182.34	84.49	3.45	0.77
T1-N30-S16	Bending-Torsion	88.84	108.84	3.24	0.99
M0-N20-S8	Pure Torsion	143.45	-	2.72	-
M0-N30-S8	Pure Torsion	129.00	-	2.44	-
T0-N20-S8	Pure Bending	-	107.97	-	0.98
T0-N30-S8	Pure Bending	-	118.78	-	1.08

Table 6 Plastic rotation limits according to different performance levels (TEC, 2018)

Performance Levels	Plastic Rotation Levels
Limited damage (LD)	$\theta_p^{(LD)} = 0$
Controlled damage (CD)	$\theta_p^{(CD)} = 0.75\theta_p^{(CP)}$
Collapse prevention (CP)	$\theta_p^{(CP)} = \frac{2}{3}\left[\left(\varphi_u - \varphi_y\right) L_p \left(1 - 0.5\frac{L_p}{L_s}\right) + 4.5\varphi_u d_b\right]$

square cross-section columns were used in this study, T-shaped cross-section columns were used in the Yu and Shan (2021) model. The difference in cross-section significantly affects the behavior under both bending and torsion effects.

In this study, 10 specimens were used, and the loads applied to each specimen were different. Therefore, the data obtained provide only limited information. Furthermore, due to the absence of direct shear-torsion stress and the simplified cantilever boundary conditions, the proposed empirical formulations have limited applicability.

3.6 Plastic rotation limits in columns

The plastic rotation limit (θ_p) defines the deformation capacity of a reinforced concrete element after it has exceeded its elastic limit. This limit is a critical parameter, particularly in performance-based assessment methods where ductile behavior is paramount. TEC-2018 is one of the regulations that directly defines this parameter for reinforced concrete columns and relates it to performance levels. These performance levels are defined as Limited Damage (LD), Controlled Damage (CD), and Collapse Prevention (CP). Table 6 provides the limit values for these performance levels defined in TEC-2018. In the formulas, φ_u represents the pre-collapse curvature of the column, φ_y represents the yield curvature, L_p represents the plastic hinge length (L_p=0.5 h), L_s represents the shear span, and d_b represents the longitudinal reinforcement diameter.

The maximum plastic rotation limit that a reinforced concrete column should exhibit varies at each performance level. These limits are used both to determine target deformations in nonlinear analyses and for performance control in linear evaluations.

In this study, performance levels corresponding to damage levels caused by horizontal loads applied to reinforced concrete columns have been determined. These levels have been compared with the limit values given in Table 6. When calculating $\theta_p^{(CP)}$ in the specimens, the φ_u and φ_y values in the equation given in Table 7 were obtained from the Bending Moment-Curvature graphs of the specimens. Section analysis was performed based on different axial load ratios to compare the performance levels of the elements with the TEC-2018 limit values, and the results are shown in Table 8. Using the analysis results, the plastic rotation limits determined for TEC-2018 based on different axial load ratios were found and compared with the test elements. While determining the plastic rotation limits, the shear span (L_s) was taken as 1200 mm and the longitudinal reinforcement (d_b) as 14 mm. For the plastic hinge lengths, the values obtained from the experiments were used.

The specimen performance was also evaluated in accordance with the ASCE/SEI 41 − 17 (2017) criteria, a key standard for the seismic assessment and retrofitting of existing buildings. Plastic rotation capacity limits are defined for rectangular columns in the standard, and in this study, θ_{pl} values were calculated for all specimens using Eqs. 14–17.

$$\frac{EI_{eff}}{EI_g} = \begin{cases} 0.3, & n \le 0.1 \\ n + 2, & 0.1 < n < 0.5 \\ 0.7, & n \ge 0.5 \end{cases} \tag{14}$$

$$\theta_y = \frac{M_{0.004} L}{3EI_{eff}} \tag{15}$$

$$\theta_{pl} = 0.042 - 0.043 \max(0.1,\ n) + 0.63\rho_s - 0.023 \max\left(0.2,\ \frac{V_y}{V_{col}}\right) \tag{16}$$

$$V_{col} = \alpha_{Col} \frac{A_{sh} f_{yw} d}{s} + \left(\frac{0.5\sqrt{f'_c}}{L/d}\sqrt{1 + \frac{N}{0.5A_g\sqrt{f'_c}}}\right) 0.8A_g \tag{17}$$

Table 7 Moment-curvature values for columns

Specimen	Yielding Curvature (rad/m)	Ultimate Curvature (rad/m)	Yielding Moment (kN.m)	Maximum Moment (kN.m)	Ultimate Moment (kN.m)
0.10 TEC (2018)	0.012	0.100	113.5	130.0	115.0
0.20 TEC (2018)	0.014	0.090	135.2	148.6	132.0
0.30 TEC (2018)	0.016	0.080	152.8	162.4	145.0
0.40 TEC (2018)	0.018	0.070	165.0	170.5	150.0
T1-N10-S8	0.013	0.066	68.1	103.5	92.8
T1-N20-S8	0.014	0.063	95.5	108.2	88.4
T1-N30-S8	0.015	0.052	75.1	91.3	73.2
T1-N40-S8	0.015	0.058	79.9	97.2	77.9
T2-N20-S8	0.012	0.036	78.2	83.5	66.8
T0-N20-S8	0.013	0.079	89.6	108.5	86.54
T0-N30-S8	0.019	0.098	105.9	121.6	97.3
T1-N30-S16	0.011	0.042	72.0	109.3	109.3

Table 8 Plastic rotation limits of specimens

Specimen	Controlled Damage $\theta_p^{(CD)}$	Collapse Prevention $\theta_p^{(CP)}$
TEC-2018 (N10)	0.0093	0.0124
TEC-2018 (N20)	0.0082	0.0109
TEC-2018 (N30)	0.0070	0.0093
TEC-2018 (N40)	0.0058	0.0078
T1-N10-S8	0.0057	0.0077
T1-N20-S8	0.0054	0.0072
T1-N30-S8	0.0042	0.0056
T1-N40-S8	0.0048	0.0065
T2-N20-S8	0.0027	0.0037
T0-N20-S8	0.0071	0.0095
T0-N30-S8	0.0086	0.0115
T1-N30-S16	0.0034	0.0046

$$\alpha_{Col} = \begin{cases} 1.0, & s/d \leq 0.75 \\ 1 - 4(s/d - 0.75), & 0.75 < s/d < 1.00 \\ 0.0, & s/d \geq 1.00 \end{cases} \tag{18}$$

(ASCE/SEI 41−17, 2017) The plastic rotation limits of the elements obtained from the tests were compared with the values calculated by ASCE-SEI (2017) and TEC (2018). The comparison results are given in Fig. 13. The results show that the plastic rotation capacity of all elements except T0-N30-S8 was well below both regulatory values.

The results of the experimental study revealed that the plastic rotation capacity of reinforced concrete columns depends on the complex interaction of torsion, axial load, and transverse reinforcement parameters. When the combined effect of these three parameters was examined, the observed changes in plastic rotation capacity generally exhibited linear behavior. In particular, the presence of torsion significantly altered the effects of the other parameters and emerged as the primary factor shaping column behavior. The plastic rotation limits for the elements, based on axial load ratios, are provided in Fig. 13.

The data presented in Table 7; Fig. 13 demonstrate that the plastic rotation capacity of reinforced concrete columns at different damage levels varies depending on axial load, torsion, and transverse reinforcement parameters.

Axial Load Effect: The decrease in the controlled damage rotation limit from 0.0093 rad to 0.0058 rad with an increase in axial load (from 0.10 to 0.40) in the regulation values is consistent with theoretical expectations. This trend has also been observed in experimental data. However, the high value of 0.0086 rad in the T0-N30-S8 indicates that the optimum axial load (0.30) can increase capacity in the absence of torsion.

Torsional Effect: It has been observed that torsion has a significant effect on the plastic rotation capacity of reinforced concrete columns. The performance differences between the T0-type specimens, which are not subject to torsion, and the torsion-subjected T1 and T2 types clearly demonstrate the extent of this effect. Comparisons at the 0.20 axial load level, in particular, show that capacity decreases significantly as torsion increases. The Controlled Damage rotation limit, which was 0.0071 rad in the T0-N20-S8 without torsion, decreased to 0.0054 rad (24% decrease) in T1-N20-S8 and to 0.0027 rad (62% decrease) in T2-N20-S8. This decrease clearly demonstrates the effect of torsion on column behavior.

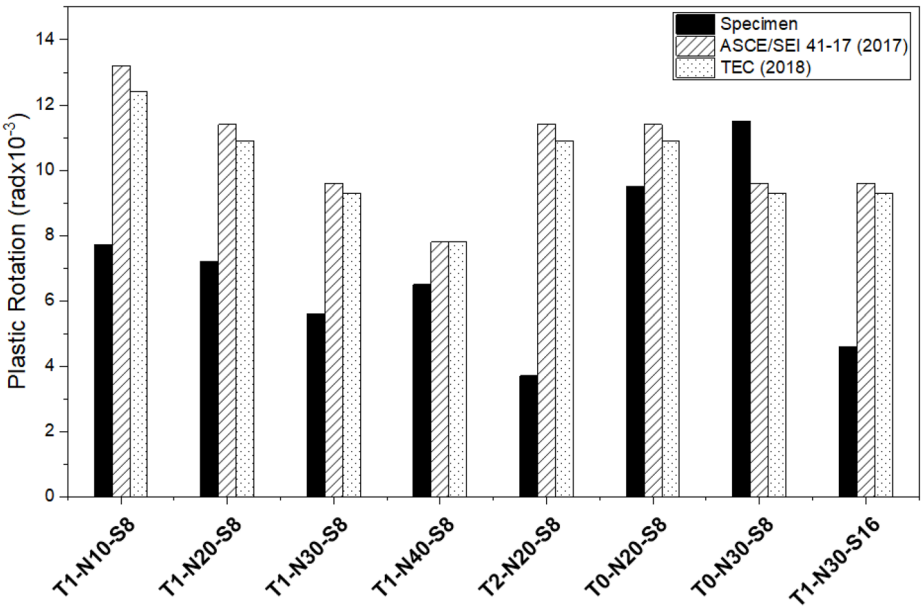

Fig. 13 Comparison of performance levels in collapse prevention

Stirrup Effect: Increasing the stirrup spacing from 80 mm to 160 mm (comparison between T1-N30-S8 and T1-N30-S16) resulted in a 19% reduction in the Controlled Damage rotation limit, decreasing it from 0.0042 rad to 0.0034 rad. This confirms the critical role of dense reinforcement in concrete confinement.

4 Conclusion

Based on experimental data, the following conclusions have been drawn:

1. The experimental results showed that torsion significantly reduced the load-carrying capacity, stiffness, displacement capacity, and energy dissipation of reinforced concrete columns. The severity of this reduction depended on the axial load level and stirrup spacing.
2. The proposed plastic hinge model incorporates the effects of torsion, axial load, and transverse reinforcement spacing. Unlike current seismic design codes, the proposed model accounts for torsion-induced damage spread. The proposed interaction model also provides a simplified representation of axial load–bending–torsion interaction in torsion-sensitive structural members.
3. The potential applications of the developed models can be evaluated across a wide range of both academic and industrial applications. From a scientific perspective, the findings of this study are expected to make a significant contribution to redefining the torsional effect in the field of earthquake engineering and to the revision of seismic design criteria. Particularly in the assessment of existing buildings in high-risk seismic zones, the

developed plastic hinge model may enable more accurate prediction of torsion-induced damage. In practical applications, engineers are expected to be able to more reliably determine the load-carrying capacities of columns under complex load combinations using the triple interaction diagram, and consequently develop more economical designs. Furthermore, it is believed that the results of this study will lay the groundwork for the development of new methodologies for structural performance evaluations and retrofitting projects and may contribute to a critical role in establishing strategies for the preservation of special structures, such as historic buildings, that are susceptible to torsion.

4. The findings of this study should be interpreted in light of several methodological and analytical constraints that define the scope and generalizability of the results. First, the empirical models proposed herein are derived from a limited dataset of ten full-scale specimens; while this represents a significant experimental effort given the complexity of three-component loading, the specimen size precludes robust statistical validation and the models should be considered preliminary, requiring independent verification with expanded experimental databases before widespread application. Second, the axial load was maintained constant throughout testing, which, while consistent with standard practice for isolating torsion effects, does not capture the P-Δ interactions and axial load variations that may occur during actual seismic events. Third, although shear-torsion interaction was evident in the failure modes of several specimens, the proposed N-M-T interaction model does not explicitly include a separate shear term, representing a simplification that future research should address. Fourth, all specimens were constructed with normal-weight concrete and conventional steel reinforcement of specific grades; the applicability of the findings to high-strength materials, lightweight concrete, or fiber-reinforced composites requires further investigation. Fifth, the cantilever boundary conditions, while representative of columns in many building frames, do not account for the rotational restraint provided by beams in actual structures, which may influence the distribution of torsional demands. Sixth, the quasi-static cyclic loading protocol, although standard for seismic behavior studies, does not fully replicate the dynamic characteristics of earthquake loading, including rate effects and multidirectional excitation. Finally, the parameter ranges investigated (axial load ratio 0.1–0.4, rotation/drift ratio 0–2, stirrup spacing 80–160 mm) define the domain within which the proposed models are valid; extrapolation beyond these ranges should be undertaken with caution. The models proposed in this study should be considered as hypothesis generators and it should be noted that the proposed plastic hinge model and interaction model are preliminary empirical models valid for the specimens used in the experimental study and under the applied loads. Despite these limitations, the systematic experimental data and the consistent trends observed provide valuable insights into the behavior of torsion-affected columns and establish a foundation for future research to build upon.

Acknowledgements This article is prepared from Salih Cengiz's doctorate dissertation entitled "The effect of axial load ratio and torsional moment on the flexural capacity of reinforced concrete columns", supervised by Prof. Dr. Mehmet Kamanli (Ph.D. Dissertation, Konya Technical University, Konya, Türkiye, 2025).

Author contributions Conceptualization: Mehmet KAMANLI; Methodology: Salih CENGİZ, Alptuğ ÜNAL, Abdulkadir SOLAK; Formal analysis and investigation: Mehmet KAMANLI, Salih CENGİZ, Alptuğ ÜNAL, Abdulkadir SOLAK; Writing - original draft preparation: Salih CENGİZ; Writing - review

and editing: Mehmet KAMANLI, Alptuğ ÜNAL, Barış BİNİCİ; Funding acquisition: Mehmet KAMANLI, Supervision: Mehmet KAMANLI, Alptuğ ÜNAL, Barış BİNİCİ.

Funding Open access funding provided by the Scientific and Technological Research Council of Türkiye (TÜBİTAK). The authors gratefully acknowledge the support provided by the Konya Technical University BAP Project named KTUN-BAP−221104022.

Data availability All data, models, and code generated or used during the study appear in the submitted article.

Declarations

Competing interests The authors declare that they have no known competing financial interests or personal relationships that could have appeared to influence the work reported in this paper.

Open Access This article is licensed under a Creative Commons Attribution 4.0 International License, which permits use, sharing, adaptation, distribution and reproduction in any medium or format, as long as you give appropriate credit to the original author(s) and the source, provide a link to the Creative Commons licence, and indicate if changes were made. The images or other third party material in this article are included in the article's Creative Commons licence, unless indicated otherwise in a credit line to the material. If material is not included in the article's Creative Commons licence and your intended use is not permitted by statutory regulation or exceeds the permitted use, you will need to obtain permission directly from the copyright holder. To view a copy of this licence, visit http://creativecommons.org/licenses/by/4.0/.

References

ACI 374.1–13 (2013) Guide for testing reinforced concrete structural elements under slowly applied simulated seismic loads. American Concrete Institute

ASCE/SEI (2017) Minimum Design Loads and Associated Criteria for Buildings and Other Structures. American Society of Civil Engineers

ASCE/SEI 41 – 17 (2017) Seismic Evaluation and Retrofit of Existing Buildings. American Society of Civil Engineers

Attarchian N, Attari NKA, Waezi Z (2020) Experimental Investigation of the Seismic Performance of Rectangular Reinforced Concrete Columns Subjected to Combined Flexure-torsion Cyclic Loading. J Earthquake Eng 26(8):3954–3976

Bach C (1890) Elastizität und Festigkeit. Die für die Technik wichtigsten Sätze und deren erfahrungsmässige Grundlage

Bae S, Bayrak O (2008) Plastic Hinge Length of Reinforced Concrete Columns. Struct J 105(3):290–300

Belarbi A, Ayoub A, Greene G, Prakash S, Mullapudi R (2007) Seismic performance of reinforced concrete bridge columns subjected to combined loading including torsion. Struct Eng Res Front 1–16

Berry MP, Eberhard MO (2008) Performance modeling strategies for modern reinforced concrete bridge columns. PEER Report 2007/07, Pacific Earthquake Engineering Research Center, University of California, Berkeley

Bishara A, Peir JC (1968) Reinforced concrete rectangular columns in torsion. J Struct Div 94(12):2913–2934

Cao X, Wu L, Li Z (2020) Behaviour of steel-reinforced concrete columns under combined torsion based on ABAQUS FEA. Eng Struct 209:109980

Cengiz S The effect of axial load ratio and torsional moment on the flexural capacity of reinforced concrete columns. Ph.D., Thesis (2025) Konya Technical University, Konya, Türkiye

Chen S, Peng W, Yan W (2018) Experimental study on steel reinforced concrete columns subjected to combined bending–torsion cyclic loading. Struct Des Tall Special Build 27(11):e1479

Coelho E, Costa AC, Candeias P, Silva MF, Mendes L (2005) Shake table tests of a 3-storey irregular RC structure designed for gravity loads. SPEAR International Workshop Proceedings (p. 123)

Coulomb CA (1784) Theoretical and Experimental Research on the Force of Torsion, and on the Elasticity of Metal Wires. M´emoires de l'Acad´emie Royale Des Sciences

Deng J, Ma ZJ, Liu A, Cao S, Zhang B (2017) Seismic performance of reinforced concrete bridge columns subjected to combined stresses of compression, bending, shear, and torsion. J Bridge Engineering 22(11):04017099

Ersoy U, Ferguson PM (1968) Concrete Beams Subjected to Combined Torsion and Shear-Experimental Trends. ACI Symp Volume Torsion ACISP–18:441–460

Ewida AA, McMullen AE (1981) Torsion–shear–flexure interaction in reinforced concrete members. Magazine Concrete Res 33(115):113–122

Feng DC, Chen SZ, Taciroglu E (2024) Deep learning-enhanced efficient seismic analysis of structures with multi-fidelity modeling strategies. Comput Methods Appl Mech Eng 421:116775

He Y, Zhang K (2020) Finite element analysis of the reinforced concrete specialshaped columns under axial force and torsion. Mater Sci Eng 892:012083

Hsu TT, Kemp EL (1969) Background and practical application of tentative design criteria for torsion. J Proc 66(1):12–23

Hsu TT, Mo Y-L (1985) Softening of concrete in torsional members-theroy and tests. J Proc 82(3):290–303

Hsu TT, Mo Y-L (2010) Unified theory of concrete structures. Wiley

Irani F, Daniali S (1993) Reinforced concrete columns in torsion. J Eng 6(4)

Jiao C, Liu Y, Wei B, Li J, Hu Z, Zhu G (2021) Seismic performance of circular reinforced concrete columns subjected to compression, bending and torsion with low and moderate shear span ratio. Archives Civil Mech Eng 21(135)

Kamanli M, Döndüren MS, Çöğürcü MT, Kekeç B, Ünal A, Saydan M, Cengiz S, Lorasokkay MA, Özdemir SA, Solak A, Nakipoğlu A (2023) Kahramanmaraş Earthquakes Hatay (Türkiye). Eğitim, Konya, Türkiye

Lessig NN (1959) Determination of the load-bearing capacity of reinforced concrete elements with rectangular cross-section subjected to flexure with torsion. Beton i Zhelezobeton 3

Mander JB, Priestley MJ, Park R (1988) Theoretical stress-strain model for confined concrete. J Struct Eng 114(8):1804–1826

Mitchell D, Collins MP (1974) Diagonal compression field theory-a rational model for structural concrete in pure torsion. J Proc 71(8)

Mullapudi TRS, Ayoub A (2013) Analysis of Reinforced Concrete Columns Subjected to Combined Axial, Flexure, Shear, and Torsional Loads. J Struct Eng 139(4):139

Nascimbene R (2015) Numerical model of a reinforced concrete building: Earthquake analysis and experimental validation. Periodica Polytech Civil Eng 59(4):521–530

Nascimbene R (2024) Investigation of seismic damage to existing buildings by using remotely observed images. Eng Fail Anal 161:108282

Navier CL (1826) R´esum´e des Lecons Donn´ees `a L'´ecole des Ponts et Chausses sur L'application de la M´ecanique `a L'´etablissement des Constructions et des Machines. Firmin Didot p`ere et Fils

Nie J, Wang Y, Fan J (2012) Experimental study on seismic behavior of concrete filled steel tube columns under pure torsion and compression–torsion cyclic load. J Constr Steel Res 79:115–126

Otsuka H, Takeshita E, Yabuki W, Wang Y, Yoshimura T, Tsunomoto M (2004) Study on the seismic performance of reinforced concrete columns subjected to torsional moment, bending moment and axial force. 3th World Conference on Earthquake Engineering No:393

Pandit GS, Mawal MB (1973) Tests of concrete columns in torsion. J Struct Div 99(7):1409–1421

Pavese A, Lanese I, Nascimbene R (2017) Seismic vulnerability assessment of an infilled reinforced concrete frame structure designed for gravity loads. J Earthquake Eng 21(2):267–289

Priestley MJ, Park R (1987) Strength and ductility of concrete bridge columns under seismic loading. Struct J 84(1):61–76

Priestley MN, Seible F, Calvi GM (1996) Seismic design and retrofit of bridges. Wiley

Rausch E (1929) Design of reinforced concrete in torsion. Technische Hochschule

Saint-Venant AJCB (1855) Memoire Sur La Torsion Des Prismes. M´emoires Pr´esent´es Par Divers Savants

Solak A (2023) Experimental investigation of the behavior of reinforced concrete columns under axial load and torsion Master's Thesis, Konya Technical University, Konya, Türkiye

TEC (2018) Turkish Earthquake Code

Timoshenko S (1905) On the stability of the flat form of bending of an I-beam under the influence of forces acting in the plane of its greatest stiffness. Bull St Petersburg Polytechnic Inst 4(3–4):151–219

Tirasit P, Kawashima K (2007) Seismic Performance of Square Reinforced Concrete Columns under Combined Cyclic Flexural and Torsional Loadings. J Earthquake Eng 11(3):425–452

Wang P, Han Qve, Du X (2014) Seismic performance of circular RC bridge columns with flexure–torsion interaction. Soil Dyn Earthq Eng 66:13–30

Wang Y-H, Wang W, Chen J (2018) Seismic behavior of steel tube confined RC columns under compression-bending-torsion combined load. J Constr Steel Res 143:83–96

Yu Z, Shan D (2021) An Experimental Study on Behaviour of Reinforced Concrete T-shaped Columns Subjected to Combined Loads. KSCE J Civ Eng 25(3):906–919
Zhou J, Chen Z, Zeng W, Liao H (2022) Seismic behavior of steel reinforced concrete column with welded studs subjected to combined action of compression-bending-shear-torsion. Eng Struct 252:113727

Publisher's note Springer Nature remains neutral with regard to jurisdictional claims in published maps and institutional affiliations.